FINAL REPORT

Time-Domain Robotic Vision Application

NASA/ASEE Summer Faculty Fellowship Program-1987

Johnson Space Center

Prepared by: C. L. Tolliver, Ph.D.

Academic Rank: Professor

University & Department: Prairie View A&M University
Electrical Engineering Department
Prairie View, Texas 77446

NASA/JSC

Directorate: Engineering

Division: Tracking and Communications

Branch: Systems Analysis Office

JSC Colleague: Kumar Krishen, Ph.D.

Date: August 14, 1987

Contract Number: NGT 44-001-800

ABSTRACT

The quest for the highest resolution microwaves imaging and the principle of time-domain imaging has been the primary motivation for recent developments in time-domain techniques. With the present new technology fast time varying signals can now be measured and recorded both in magnitude and in phase. It has also enhanced our ability to extract relevant details concerning the scattering object.

In the past, the inference of object geometry or shape from scattered signals has received substantial attention in radar technology. Various inverse scattering theories were proposed to develop analytical solutions to this problem. Furthermore, the random inversion, frequency swept holography, and the synthetic radar imaging, all of which have two things in common: (a) the physical optic far-field approximation and (b) the utilization of the channels as an extra physical dimension, were also advanced significantly.

Despite the inherent vectorial nature of electromegnetic waves, these scalar treatments have brought forth some promising results in practice with notable examples in subsurface and structure sounding. The use of time-domain imaging for space robotic vision applications has been proposed. A multisensor approacah to vision has been shown to have several advantages over video-only approach.

FINAL REPORT

OBJECTIVES

The continued research efforts for this project should be as follows: (1) develop the application of time-domain imaging for robotic vision, in order to emphasize this we stress that it is the scattered field not the total power that is of interest; (2) research the hardware/technology needed for this application; (3) derive theoretical expressions for planar, cylindrical, spherical, and octobox configurations (the images will be synthesized on the basis of time-domain reflectance); (4) study the effects of pulse width, polarization, look angle, and carrier frequency and (5) compute magnitude and phase images. The limitations of the present analytical techniques will be identified. Also, experimental verification of the analytical results will be performed to develop hardware approaches.

INTRODUCTION

The detailed literature review conducted this summer at the Johnson Space Center, in the area of Time-domain microwave target imaging, led to a research topic of determining the size, shape, and electromagnetic properties of a scatter, given the incident and scattered eletromagnetic fields. The problem of interest here is the reconstruction of the shape of a convex scatter from knowledge of high frequency far field scattered from the object in response to a known incident field.

The quest for the highest resolution microwaves imaging and the principle of time-domain imaging has been the primary motivation for recent developments in time-domain techniques. In the last decade, modern techniques in sampling devices and advent of fast pulse generators has brought new technology to the practicing radar engineers in the measurements of picosecond at a much reduced cost. With the present new technology fast time varying signals can now be

measured and recorded both in magnitude and in phase.

Todays technology has enhanced our ability to extract relevant details concerning the scattering object, which conventional radar ranging lacks.

In the past, the inference of object geometry or shape from scattered signals has received substantial attention in radar technology largely due to its adademic significance and the understandable commercial and military values. In the last decade various inverse scattering theories were proposed to develop analytical solutions to this problem. Furthermore, the random inversion, frequency swept holography, and the synthetic radar imaging, all of which have two things in common:

(a) The physical optic far-field approximation.

(b) The utilization of the channels as an extra physical dimension, were also advanced significantly.

Despite the inheret vectorial nature of electromagnetic waves, these scalar treatments have brought forth some promising results in practice with notable examples in subsurface and structure sounding. Recently Dr. Kumar Krishen, of NASA/JSC, has proposed the use of time-domain imaging for space robotic vision applications. A multisensor approach to vision has been shown to have several advantages over video-only approach.

PROBLEM

(THEORETICAL APPROACH)

The problem of scattering from rough surfaces is inherently different in nature from that of scattering by other bodies. Usually in the rough-surface problem, an exact knowledge of the shape of the surface is neither available, nor is it of interest to the radar operator. Instead, only average properties of the surface shape enter into the problem. It is clearly understood that the last requirement rule out a boundry-value approach, since the exact boundry is not known. We are more interested in the relationship between the average scattered

field or radar cross section and the average surface properties. The radar cross section is normalized by the area A, and defined as, $\gamma(\theta_i, \theta_s, \varphi_s) = \langle\sigma(\theta_i, \theta_s, \varphi_s\rangle/A$, where the three angles θ_i, θ_s, and φ_s are shown for bistatic case in figure 1a below. The rough surface is assumed to consist of height variations about a mean plane, which is taken as the xy-plane. The incident wave lies in the xz-plane at a polar angle.

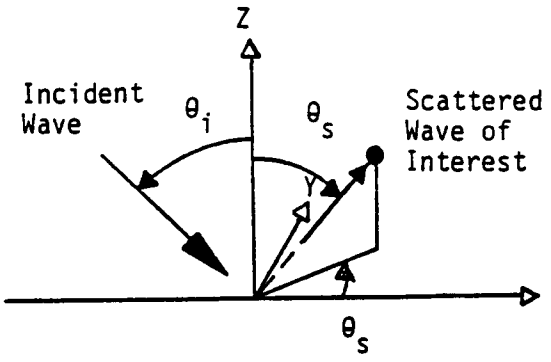

Figure 1a - BISTATIC SCATTERING GEOMETRY

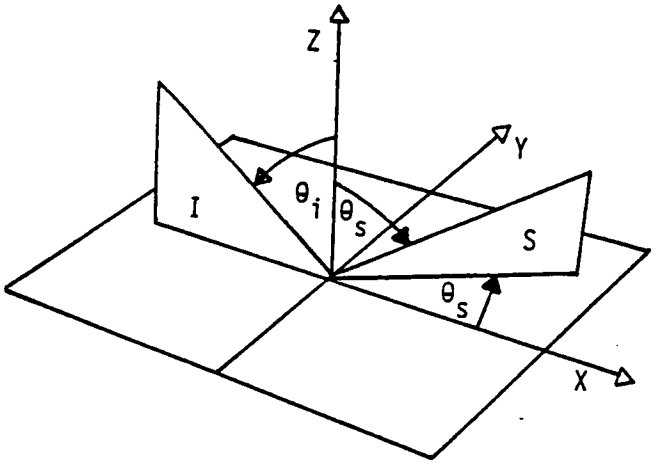

Figure 1b - THE "SCATTERING GEOMETRY"

Figure 1a shows the bistatic scattering for a planar rough surface whose mean

height coincides with the xy-plane and figure 1b shows the scattering geometry. I is the plane of incidence and S is the scattering plane.

The < > refer to an average. For the normaized average backscattering cross section are defined as

$$\gamma(\varepsilon_i) = \gamma(\varepsilon, \varepsilon, \pi)$$

Generally one has specific purposes or reasons for investigating scattering from a rough surface broadly these ultimate goals may be divided into three categories:

(1) The problem of direct scattering; one wishes to know the average properties of the scattered signal or cross section when the surface properties of the rough surface are known, and the scattering information is expressed in terms of the surface properties.

(2) The problem of inverse scattering; one wishes to obtain statistical information about the rough surfaces from a knowledge of the average properties of the scattered field. This problem is more difficult in that there appear to be many classes of rough surfaces producing the same average scattering cross section as a function of the bistatic scattering angle and wavelength.

The (scattered field) radar cross section, can be expressed as 4π times the power delivered per unit solid angle in the direction of the receiver divided by the power per unit area incident at the target. The factor 4π enters from the definition of solid angle. Assuming for the moment that the propagation path between the target and the receiving system is lossless, then this power ratio may be expressed as

$$4\pi r^2 (\Xi^s \cdot \Xi^{s*}) / (\Xi^i \cdot \Xi^{i*}) = 4\pi r^2 (\Xi^s \cdot \Xi^{s*}) / (\Xi^i \cdot \Xi^{i*})$$

where E^S and H^S are the scattered electric and magnetic fields, respectively and

E^i and H^i are the incident fields. The scattered field is defined to be the difference between the total field (with the targety present) and the incident field E^i (the total field that would exist if there were no target present). This is summarized as $E^S = E^T - E^i$.

Finding the cross section (σ) now becomes a problem in electromagnetic field theory. In order that the cross section be independent of r, it is desirable to let r in (Eg. 3) become arbitrarily large (scalar definition, not a tensor function).

$$\sigma = 4\pi \lim_{r\to\infty} r^2 (E^s \cdot E^{s*})/(E^i \cdot E^{i*}) = 4\pi \lim_{r\to\infty} r^2 (H^s \cdot H^{s*})/(H^i \cdot H^{i*})$$

To compute the scattered field one sometimes computes the current induced on the target and then treats the target current distribution in terms of an equivalent aperature distribution. Antennas are often compared to an isotropic antenna, that is, an antenna which radiates uniformly in all directions.

In the clutter problem, return from terrain is not wanted. However, in many cases the presentor clutter is unavoidably along with the desired signal, one can detect and analyze the desired signal significantly if more is known about the properties of the clutter or noise produced by terrain scattering. It is noted that surface information is generally known, and the properties of the scattered signal are sought related to (Eq. 3). At this point in time, a few more mathematical definitions may be of interest.

The source signal is related to the Fourier transform, F(w), by:

$$\text{(a) } F(w) = \int_{-x}^{x} f(t)e^{jwt}\,dt, \qquad \text{(b) } f(t) = \frac{1}{2\pi}\int_{-x}^{x} F(w)e^{-jwt}\,dt$$

Known by the Fourier transform pair as follows:

$$\text{(a) } F(w) = \int_{-\infty}^{\infty} f(t)e^{jwt}\,dt, \qquad \text{(b) } f(t) = \frac{1}{2\pi}\int_{-\infty}^{\infty} F(w)e^{-jwt}\,dt$$

Capitals are used to denote transformed function unless otherwise noted or stated. The wave number k = w/c, where c is the speed of light in the medium. α and β are the direction cosines of the vector r projected onto the xy-plane (with $\alpha = \sin\xi\cos\xi$, $\beta = \sin\xi\sin\xi$).

It can be assumed that the field distribution over the antenna apertures and object plane is space - time separable; the field strength of each radiating element observed at some point r is $e(r,t) = e(r)f(t-\frac{r}{c})$ the field strength. Where $f(t-\frac{r}{c})$ is the sine wave traveling at the speed of light.

Consider the scatter in figure 2 to be placed in a far field, such that the assumption of a uniform impinging planewave over the object can be assured. The incident wave form i(t), on the object surface is obtained by the application of the far field Kirchhoff-Huygens principle, namely

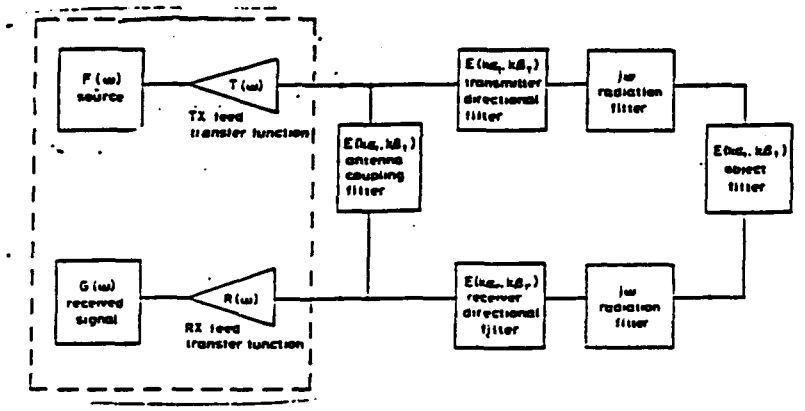

Figure 2.- SCHEMATIC DIAGRAM OF THE TARGET IMAGING SYSTEM

Let P be a point of observation and let R' be the distance from P to a point $\xi(x,y)$ on the surface S. The scattered field E at P is given by the Helmholtz integral as follows:

$$E(p) = \frac{1}{4\pi} \oint_s \left(E\frac{\partial \psi}{\partial n} - \psi\frac{\partial E}{\partial n}\right)ds$$

Let V be a volume bounded by a surface S and let A be any continuous vector function. Then, according to the divergency theorem,

$$\iiint_v \nabla \cdot A\,dv = \oint_s A \cdot n\,ds$$

Green's First Theorem:

$$\iiint_v \nabla E \cdot \nabla \psi\,dv = \oint E\frac{\partial \psi}{\partial n}ds - \iiint_v E\nabla^2\psi\,dv$$

Green's Second Theorem:

$$\iiint_v (E\nabla^2\psi - \psi\nabla^2 E)dv = \oint_s \left(E\frac{\partial \psi}{\partial n} - \psi\frac{\partial E}{\partial n}\right)ds$$

Note, the scattered field E(p) at the point of observation is given by the Helmholtz integral as follows:

$$E(p) = \frac{1}{4\pi}\oint_s \left(E\frac{\partial}{\partial n}\frac{e^{jkr}}{r} - e^{jkr}\frac{\partial E}{\partial n}\right)ds$$

(To get a better mathematical understanding of the application on how the scattered wave form is obtained, please refer to the author on the derivation of the scattered wave of interest in frequency domain).

$$I(w) = \frac{\cos\theta}{4\pi r_0} jwF(w)\int_x^x \int e(x,y)\exp\{-jk(r_0 - \alpha_x - \beta y)\}\,dxdy$$

$$I(w) = \frac{\cos\theta}{4\pi r_0} jwF(w)T(w)E_t(k\alpha_t, k\beta_t)\exp\{-jkr_0\}$$

Where $E_t(k\alpha_t, k\beta_t)$ is the transmitting-antenna anisortopic directional

filter and r is the distance between the transmitter aperture and an object plane taken as reference.

By stationary - phase evaluation and a second application of the Kirchhoff-Huygens principle, it can be shown, with little algebra that the received waveform, g(t), is

$$g(t) = \text{const}\int_{-\infty}^{\infty} F(w)T(w)R(w)[E_c(k\alpha_c, k\beta_c) + (jw)^2 E_1(k\alpha_1, k\beta_1)E_2(k\alpha_2, k\beta_2)E_0(k\alpha_0, k\beta_0)e^{-jkr}\,dw$$

For the monostatic case commonly encountered (see figure 3 below), the transmitter and receiver coincide. In particular, if the phase center of the object is on boresight which suggests that the target is closely tracted, eqr.16 can be considerably simplified to yield:

$$g(t) = \text{const}\int_{-\infty}^{\infty} F(w)T(w)R(w)[E_a(k\alpha_c, k\beta_c) + (jw)^2 E_1(0,0)E_2(0,0)E_0(k\alpha_0, k\beta_0)e^{-jwt}\,dw$$

The delineation of the object response is exercised as follows: First, the time response in the absence of any scattering objects is recorded.

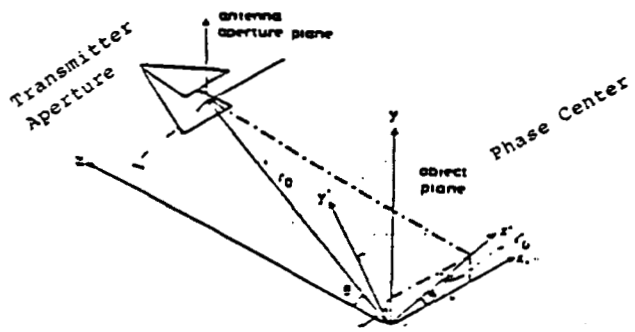

(a) $X = \dfrac{\partial x' + \beta y'}{\sqrt{\partial^2 + \beta^2}}$ (b) $y = \dfrac{\beta x' - \partial y'}{\sqrt{\partial^2 + \beta^2}}$

(c) $\text{Cos}\,\phi = \dfrac{\partial}{\sqrt{\partial^2 + \beta^2}}$ (d) $\text{Sin}\,\phi = \dfrac{\beta}{\sqrt{\beta^2 + \partial^2}}$

Figure 3 - IMAGING GEOMETRY

THE ROTATION TRANSFORMATION

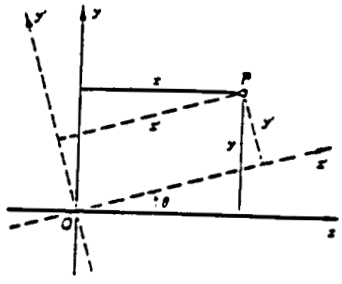

FIGURE 3a.

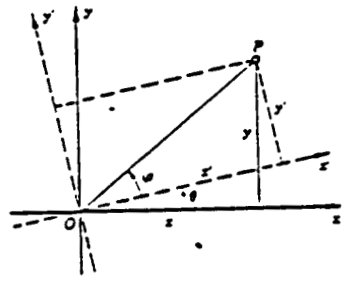

FIGURE 3b.

(f) $x = x' \cos\theta - y' \sin\theta,$
$y = x' \sin\theta + y' \cos\theta,$

(g) $x' = x \cos\theta + y \sin\theta,$
$y' = -x \sin\theta + y \cos\theta.$

(h) $\frac{x}{|OP|} = \cos(\varphi + \theta),$
$x = |OP| \cos(\varphi + \theta)$
$= |OP| (\cos\varphi \cos\theta - \sin\varphi \sin\theta).$

(i) $\sin\varphi = \frac{y'}{|OP|}$ and $\cos\varphi = \frac{x'}{|OP|}$

This signal is subsequently substracted from other records with the scatter present, thus removing the antennas coupling filter. Given a sufficiently large free space, multiple path scattering between the object and surrounding obstacles can be gated out in time. By definition

$$\Xi_0(k\alpha_0, k\beta_0) = \int_{-\infty}^{\infty}\int e(x,y)\exp[+jk(\alpha_0 x + \beta_0 y)]\,dx\,dy$$

Having removed the coupling term, the backscattering waveform g(t), gives the

system kernel, K(w),

$$K(w) = \cos t + (jw)^2 F(w)T(w)R(w)\Xi_r(0,0)\Xi_r(0,0)e^{-2jkr_0}$$

with the use of mathematical techniques, the backscattering waveform was simplified, to give the system kernel, K(w), further giving an opportunity to obtain the electric field strength in frequency domain

and by the Projection theorem , the response obtained is equivalent to a slice in the two dimension fourier plane (Figure 4).

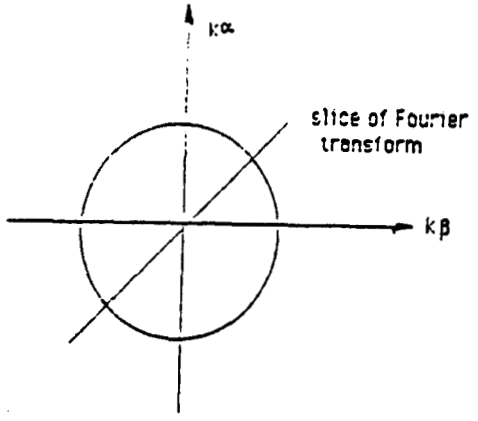

Figure 4. - REPRESENTATION OF THE ONE-DIMENSIONAL TARGET FREQUENCY RESPONSE IN THE TWO-DIMENSIONAL FOURIER PLANE AT A PARTICULAR VIEWING DIRECTION

It is further noted that the help of figures 3a, 3b assisted in a change in spatial coordinates in Figure 3 from one dimension coordinate system to the two dimension coordinate system $\Xi(k\alpha, k\beta)$.

Followed by an inverse fourier transform (Eq. 11) yields the object impulse response $\int_{-\infty}^{\infty} \Xi(k,o)e^{-jw(t-2x'\sin\frac{\xi}{c})}dw = e(t - 2x'\sin\frac{\xi}{c})$

which can be considered as a series of scans across the object surface where each is an integral of the object field which is orthogonal to the viewing direction. The spatial resolution is thus achieved by the utilization of the time channel and the minimal resoluable dimension Δx is related to the sampling integral T, namely $\Delta x = \frac{c\pi}{2\beta \sin\theta}$

The two-dimensional object field distribution is recovered, namely the reconstruction field strength, e(x,y)

$$e(x,y) = \frac{1}{4\pi^2} \int_0^{\pi} \int_{-\infty}^{\infty} \Xi(k\alpha, k\beta) A(k\alpha, k\beta) e^{j k(\alpha x, \beta y)} k d\alpha d\beta$$

a smoothing filter $A(k\alpha, k\beta)$ is introduced to compensate due to the factor k in the field strength equation $e_0(x,y)$. It is not necessary to have A, for noise free data. For practical numerical evaluation, the finite sampling rate will impose an upper limit, R, to the wave number k. To eliminate abrupt cutoff which would cause ringing in the resultant image, it is necessary to introduce

$$A(k\alpha, k\beta) = \sin\left(\frac{k\pi}{2R}\right) / \left(\frac{k\pi}{2R}\right)$$

which yields a smoothed image

$$e(x,y) = \frac{1}{4\pi^2} \int_0^{\pi} d\beta \int_{-R}^{R} \frac{k}{2} \Xi(k\alpha, k\beta) \sin\left(\frac{k\pi}{2R}\right) e^{j k(\alpha x, \beta y)} dk$$

and is the basis of our reconstruction field strength.

RESULTS

Theoretical calculations of the single and train pulse of the schematic diagram (figure 2) of the target imaging sytem led me to analyze fourier transform of the input function. A program was written in Basic and the use of BOSS (Block Oriented System Simulator) enable me to plot the energy supplied to the target and give the time plot of a single and train of pulses. I was also able to verify the magnitude spectrum of a single pulse continuous descrete function and the magnitude spectrum of a line spectrum of pulse train.

APPLICATIONS

- Recently NASA/Johnson Space Center has proposed the use of time-domain imaging for Space Robotic vision applications.

- Many space objects are covered with heat shields, etc. (Dielectric Materials) and microwave can sense through this layer.

- A multisensor approach to this vision has been shown to have several advantages over video-only approach.

RECOMMENDATIONS

- It is recommended that the second phase of the research project, inititated at the NASA/Johnson space Center, in the area of Time-Domain Robotic Visions Applications, be continued to study the effects o9f pulse width, polarization, look angle, and phase images on robotic vision, and to conduct experiments to verify the theoretical results.

- The amount of time provided for the theoretical and experimental verification of the Time-Domain Microwaive Robotic Vision Application was not sufficient in order to perform the above experimental verification.

$$|F(w)|^2 = \frac{\pi^2}{\tau_0^2}\left[\frac{1}{\omega}+\sum_{n=1}^{\infty}\frac{\sin\frac{n\pi}{\tau_0}}{\frac{n\pi}{\tau_0}}\,\frac{\omega}{\omega^2-\left(\frac{n\pi}{\tau_0}\right)^2}\right]\left[\frac{1}{\omega}+\sum_{n=1}^{\infty}\frac{\sin\frac{n\pi}{\tau_0}}{\frac{n\pi}{\tau_0}}\,\frac{\omega}{\omega^2-\left(\frac{n\pi}{\tau_0}\right)^2}\right]$$

```
LIST
5 PRINT "The Energy Supplied To The Target is |F(w)|^2 = F(w)F(w)*"
6 PRINT
7 PRINT
8 PRINT "|F(w)|^2="
9 PRINT
10 FOR N = 1 TO 4
15 PRINT  "N","w","F(w)F(w)*"," B",
16 PRINT
20 FOR W = 5 TO 10
30 B = (2/( N * 3.14 ))* (SIN (N * .0314)) * (W/( W*W - N*2*3.14)/EXP(10-10))
35 FW = ( 1 /( 2 * 3.14)* (.01))+ B * (1/(2*3.14) *(.01))-B
60 PRINT  N,W,FW,B
70 NEXT W
80 NEXT N
O
```

```
RUN
The Energy Supplied To The Target is |F(w)|^2 = F(w)F(w)*

|F(w)|^2=

N             w             F(w)F(w)*                B
 1             5             6.941864E-03             5.341003E-03
 1             6             5.635806E-03             4.037021E-03
 1             7             4.874189E-03             3.276615E-03
 1             8             4.368317E-03             2.771547E-03
 1             9             4.004789E-03             2.408598E-03
 1             10            3.729419E-03             2.133665E-03
N             w             F(w)F(w)*                B
 2             5             9.63845E-03              8.033302E-03
 2             6             6.716592E-03             5.116089E-03
 2             7             5.437877E-03             3.839407E-03
 2             8             4.705682E-03             3.108376E-03
 2             9             4.224854E-03             2.628312E-03
 2             10            3.881775E-03             2.285779E-03
N             w             F(w)F(w)*                B
 3             5             1.782794E-02             1.620977E-02
 3             6             8.586145E-03             6.982669E-03
 3             7             6.234785E-03             4.635048E-03
 3             8             5.135711E-03             3.537721E-03
 3             9             4.488433E-03             2.891472E-03
 3             10            .0040569                 2.460625E-03
N             w             F(w)F(w)*                B
 4             5             -.8308692                -.8311381
 4             6             1.261031E-02             1.100044E-02
 4             7             7.448911E-03             5.847244E-03
 4             8             5.703307E-03             4.104415E-03
 4             9             4.810195E-03             3.212726E-03
 4             10            4.260522E-03             2.663923E-03
O
```

Table I - The Energy Supplied To the Target

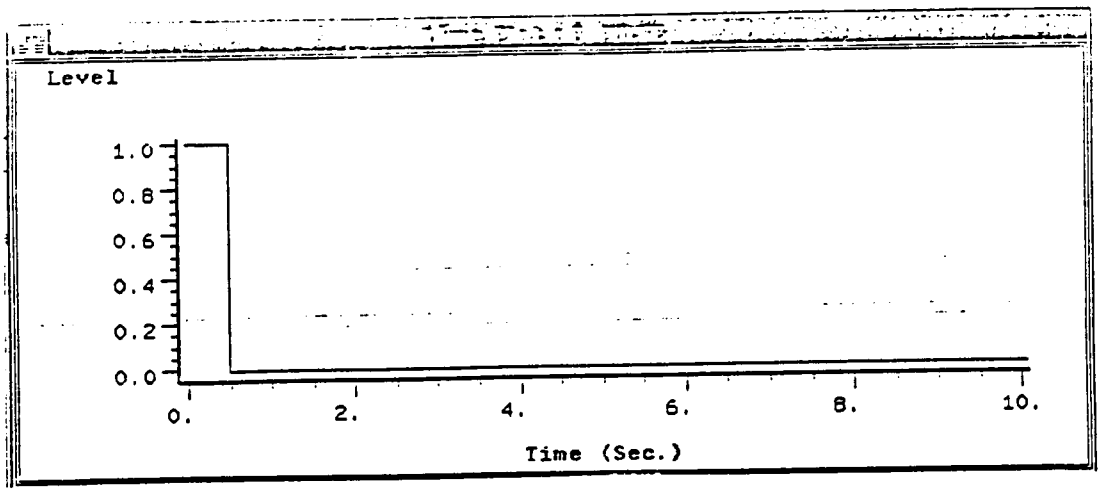

Figure 5.- Time Plot of a Single Pulse

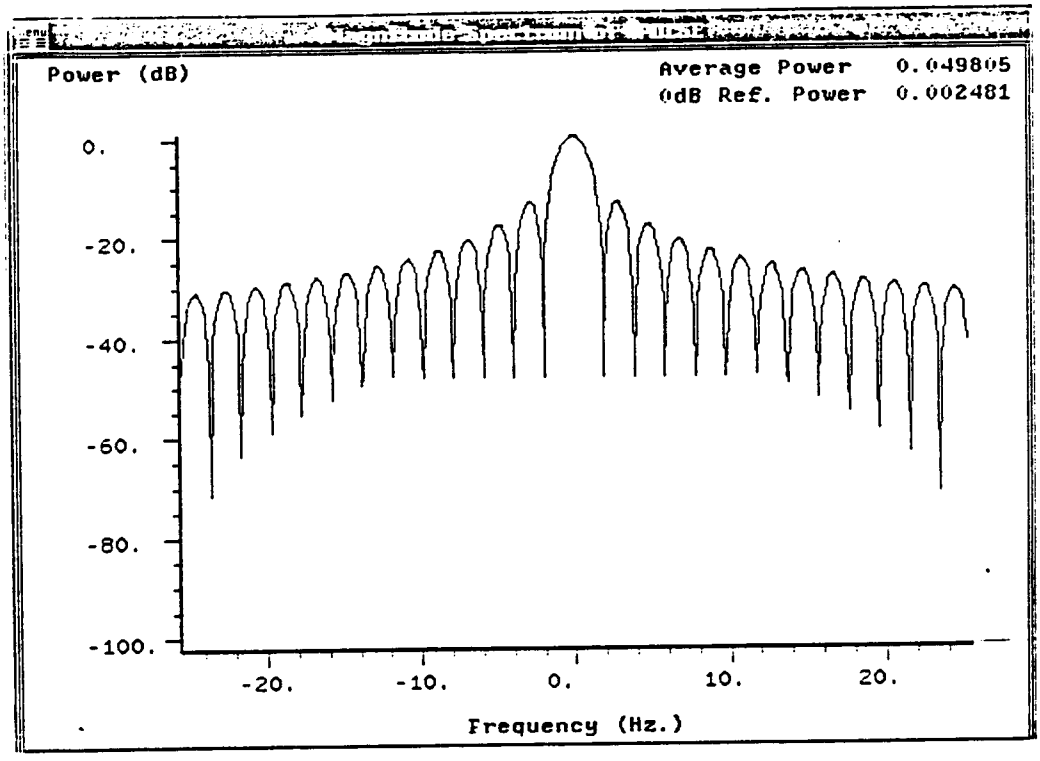

Figure 6.- Magnitude Spectrum of a Single Pulse

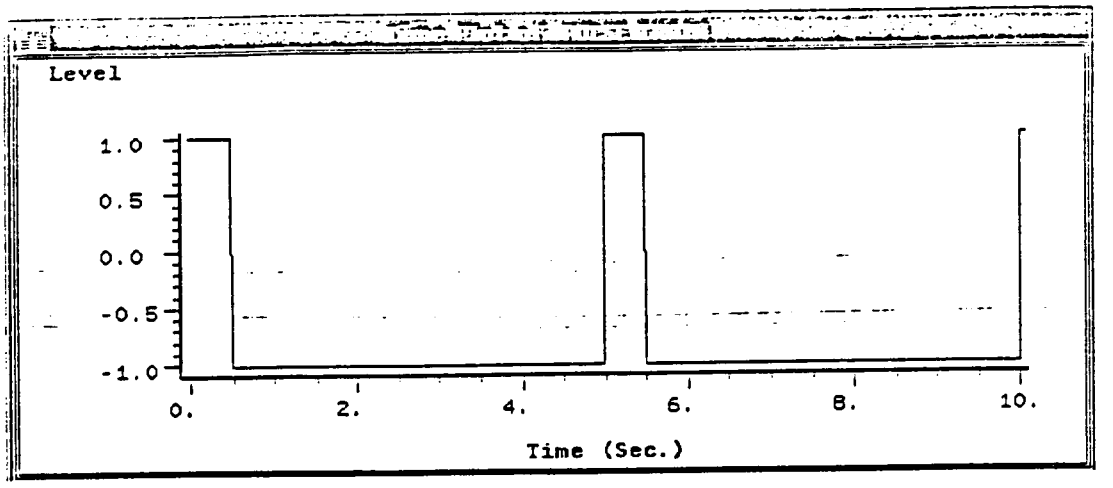

Figure 7.- Time Plot of A Pulse Train

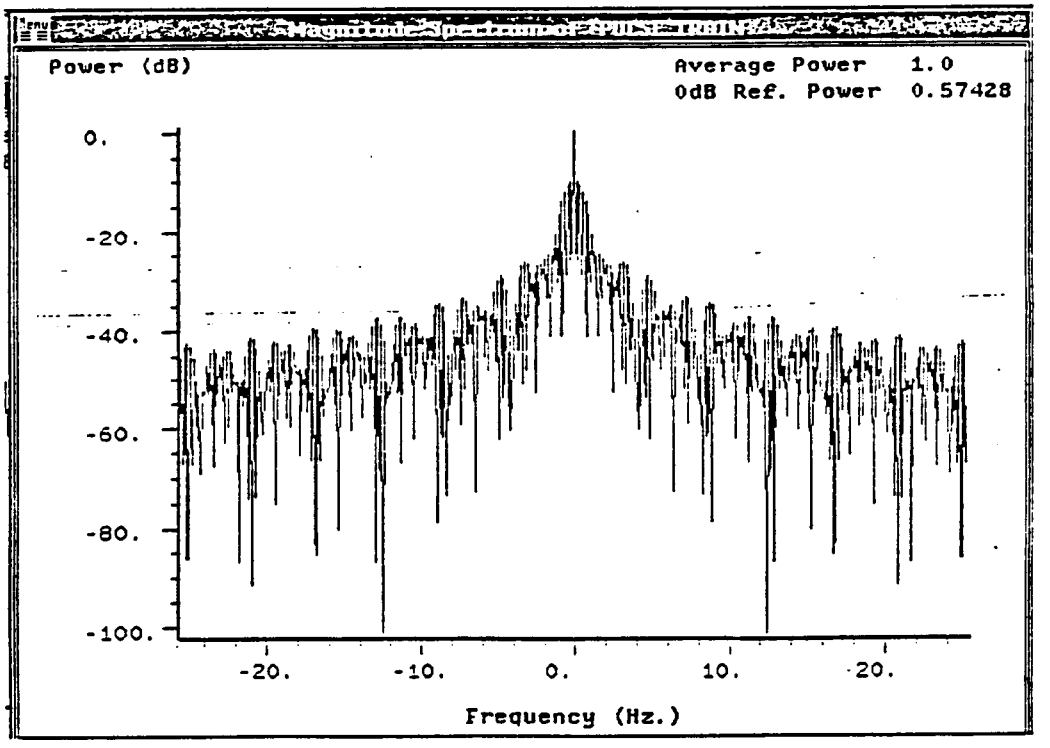

Figure 8.- Magnitude Spectrum of A Pulse Train

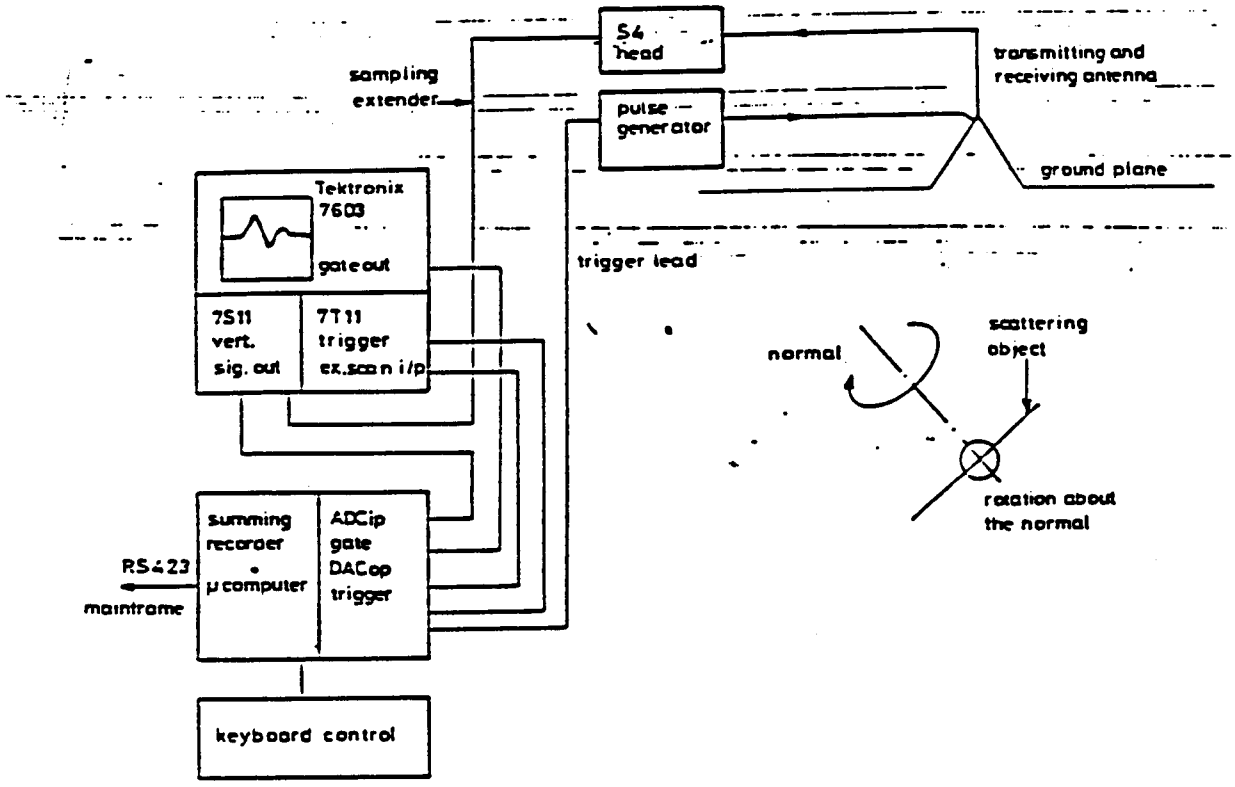

Figure 9.- Experimental Arrangement of the Target Scattering Measurement

The above is a circuit diagram which will be used to verify the results of elliptical and bowtie geometry of targets (Figures 10, 11, 12, and 13)

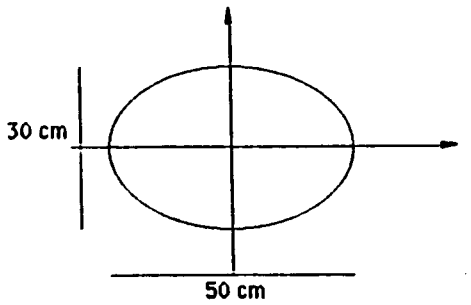

Figure 10- Geometry of the elliptical target.

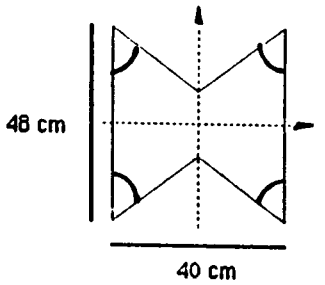

Figure 12- Geometry of the Targets - Bow-Tie

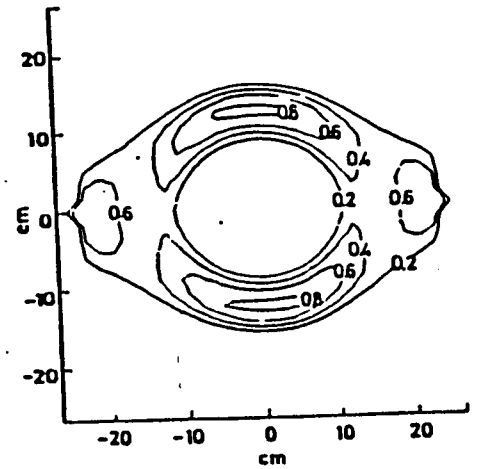

Figure 11- Reconstructed Images -Ellipse

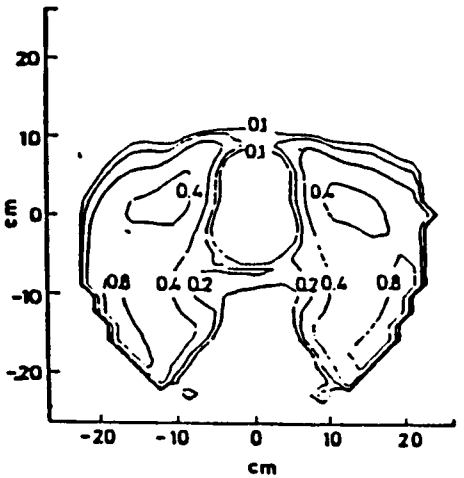

Figure 13- Reconstructed Images - Bow-Tie

ACKNOWLEDGEMENT

This research was conducted under the direction of Dr. Kumar Krishen and the Tracking and Communications Division (TCD). I also enjoyed discussions and interaction with several TCD personnel including James E. Ratliff, Ricardo J. Villarreal, Budy J. Walker and Ned J. Robinson. The encouragement of Mr. R. S. Sawyer, Chief, TCD is greatly acknowledged. Special acknowledgement to Ms. Michelle K. Morris for her typing support.

BIBLIOGRAPHY

Bachman, C.G.: Radar targets(Gover Pub. Co. Ltd., 1982), pp. 110-113.

Beckman, P. and Spizzichino, A.: The Scattering of Electromagnetic Waves from Rough Surfaces(The Macmillan Co., 1963), pp. 10-28, 178-181.

Bennett, C.L., and Ross, G.F.: Time domain electromagnetics and its applications, ibid., 1978, 66, pp. 299-318.

Boerner, W.M., HO, C.M., and Foo, B.Y.: Use of Radon's projection theory in electromagnetic inverse scattering, IEEE Trans., 1981, AP-29, pp, 336-341.

Chan, C.K., and Farhat, N.H.: Frequency swept tomographic imaging of three dimensional perfectly conducting objects, ibid, 1981, AP-29, pp. 312-319.

Censor, Y.: Finite series-expansion reconstruction methods, ibid, 1983, 71, pp. 409-419.

Evans, S., and Kong, F.N.,: Gain and effective area of impulse antenna, Third International Conference on Antenna and Propagation, ICAP 83, Norwich, England, April 1983, pp. 421-424.

Fialkovskiy, A.T.: Diffraction of planar electromagnetic waves by a slot and a strip, Radio Eng. Electron., 1966, 11, pp. 150-157.

Kennaugh, E.M. and Moffatt, D.C.: Transient and impulse approximations, Proc. IEEE, 1965, 53, pp. 893-901.

Kong, F.N.: Ph.D. Dissertation, Cambridge University, August 1983, Chap. 8.

Lewitt, R.M.: Reconstruction algorithms: transform methods, Proc. IEEE, 1983, 71, pp. 390-408.

Reader, H.C., Evans, S., and Yeaung, W.K.: Illumination of a rectangular slot radiator over a 3 Octave bandwidth, Fourth International Conference on Antennas and Propagat., ICAP 85, 1985, pp. 223-226.

Ruck, G.T., Barrick, D.E., Stuart, W.D., and Krichbaum, C.K.: Radar Cross Section Handbook(Plenum Press, 1970), pp. 671-689.

Schubert, K.A., Young, J.D., and Moffatt, D.L.: Synthetic Radar imaging, ibid, 1977, AP-25, pp. 477-483.

Tikhonov, A.N. and Arsenic, V.Y.: Solutions of ill-posed problem (Winton-Wiley, New York, 1977).

Yeung, W.K. and Evans, M.A.: Time-domain microwave target imaging, Proc. IEEE, 1985, 132, pp. 345-350.